



Article

Highly Efficient Visible-Light-Driven Photocatalysis of Rose Bengal Dye and Hydrogen Production Using Ag@Cu/TiO₂ Ternary Nanocomposites

Satish Yadav ¹, Asim Jilani ², Sarika Sachan ¹, Pramod Kumar ^{1,*}, Sajid Ali Ansari ³, Muhammad Afzal ⁴ and Mohammad Omaish Ansari ^{2,*}

- Functional Materials Laboratory, Department of Chemistry Prof. Rajendra Singh (Rajju Bhaiya), Institute of Physical Sciences for Study and Research, Veer Bahadur Singh Purvanchal University, Jaunpur 222003, Uttar Pradesh, India; sarikasachan27aug@gmail.com (S.S.)
- ² Center of Nanotechnology, King Abdulaziz University, Jeddah 21589, Saudi Arabia; asim.jilane@gmail.com
- Department of Physics, College of Science, King Faisal University, P.O. Box 400, Al-Ahsa 31982, Saudi Arabia; sansari@kfu.edu.sa
- Department of Pharmaceutical Sciences, Pharmacy Program, Batterjee Medical College, P.O. Box 6231, Jeddah 21442, Saudi Arabia; mohmmad.afzal@bmc.edu.sa
- * Correspondence: pkchemistry.2009@gmail.com (P.K.); moansari@kau.edu.sa (M.O.A.)

Abstract: In this work, an Ag@Cu/TiO₂ ternary nanocomposite was synthesized by a simple chemical methodology and subsequently studied for the photocatalytic degradation of rose bengal (RB) dye under visible light as well as its hydrogen production. The shape, size and topographical analysis by scanning and transmission electron microscopy revealed that all the constituents are well intercalated and are in the nano range. The energy dispersive X-ray analysis of the Ag@Cu/TiO2 showed the presence of Ti, O, Cu and Ag and the absence of any other impurities, while the mapping analysis showed their uniform distribution. The X-ray photon spectroscopy also showed successful interaction between the components. Furthermore, the changes in the chemical state of Ti2p were examined. The band gap of Ag@Cu/TiO2 using the Tauc plot relations was found to be the lowest at 2.86 eV in comparison to pure TiO₂ (3.28 eV), binary Ag/TiO₂ (3.13 eV) and Cu/TiO₂ (3.00 eV). The Ag@Cu/TiO₂ displayed the lowest photoluminescence intensity, suggesting the highest degradation efficiency and lowest recombination rate. The application of Ag@Cu/TiO2 toward the photocatalytic degradation of RB dye exhibited a degradation rate of ~81.07%, which exceeds the efficiency of pure TiO₂ by 3.31 times. Apart from this, the hydrogen production of Ag@Cu/TiO₂ was found to be 17.1 µmol h⁻¹ g⁻¹, suggesting that copper and silver synergistically contributed, thereby resulting in the increased hydrogen production of pure TiO₂.

Keywords: rose bengal dye; visible region; photocatalytic degradation; Ag@Cu/TiO₂ ternary nanocomposites



Citation: Yadav, S.; Jilani, A.; Sachan, S.; Kumar, P.; Ansari, S.A.; Afzal, M.; Ansari, M.O. Highly Efficient
Visible-Light-Driven Photocatalysis of Rose Bengal Dye and Hydrogen
Production Using Ag@Cu/TiO2
Ternary Nanocomposites. Chemistry
2024, 6, 489–505. https://doi.org/
10.3390/chemistry6030028

Academic Editors: Gianguido Ramis, Vincenzo Vaiano and Olga Sacco

Received: 15 April 2024 Revised: 29 May 2024 Accepted: 30 May 2024 Published: 20 June 2024



Copyright: © 2024 by the authors. Licensee MDPI, Basel, Switzerland. This article is an open access article distributed under the terms and conditions of the Creative Commons Attribution (CC BY) license (https://creativecommons.org/licenses/by/4.0/).

1. Introduction

Water is an essential element for the survival of life on the Earth and is present on the Earth in the form of rivers, seas, lakes and ground water. The rapid growth of the population, development, Industrial Revolution, and climate change have contaminated every aspect of water resources [1]. The main contaminants in water are tannery, leather, rubber, dyes, cosmetics, food pharmaceuticals, printing paint, etc. [2,3]. Among them, textiles, pharmaceuticals, printing paints and fabric industries discharge colored dye up to 17–20% into water bodies, which has created water pollution [4]. Synthetic colored dyes are non-biodegradable and highly photostable [5]. The dye inhibits sunlight, decreases the solubility of molecular oxygen in water, which affects the aquatic life of organisms as well as the ecosystem of water, and has long-term toxic and carcinogenic effects for all ecosystems.

Among the most widely used organic dye is rose bengal (RB) dye, which is used in the textiles, printing, and cosmetic photochemical industries. It must be removed from water since it causes itching, redness, inflammation, irritation, and blistering when it comes into direct contact with skin. Different methods, including membrane filtration, coagulation, flocculation, and adsorption, have recently been used to degrade dye pollution [6–8]. However, all these methods have limitations, including effluent, sludge development, and difficulty reactivating the adsorbent. Photocatalysis is one of a most common and most cost-effective methods to decompose RB dyes from water using efficient nanocatalysts [9]. Visible light photocatalysis is a process that utilizes the energy from visible light to initiate a chemical reaction. It involves the use of a photocatalyst, which can absorb light in the visible spectrum and promote the conversion of reactants into the desired product [10]. Recently, this technique has drawn a lot of interest owing to its environmental friendliness, versatility, selectivity, efficiency, cost-effectiveness and sustainability, which make it highly applicable for a large number of uses.

Nanoparticles show different properties to the bulk materials or molecular species or atoms from which they are derived due to the high surface volume ratio [11]. The various types of nanoparticles of transition metals [12], transition metal oxides and chalcogenides are used for varied applications, such as energy storage, magnetic data storage, sensors, and ferrofluids, and photocatalytic degradation of organic dye. Nanoparticles, particularly metal oxide nanoparticles, are widely used in the field of visible light photocatalysis. These nanoparticles have unique properties that make them effective in photocatalysis for various reactions. For instance, metal oxide nanoparticles such as titanium oxide (TiO₂) [13], zinc oxide (ZnO) [14], and tungsten oxide (WO₃) [15] have been extensively studied for their photocatalytic capabilities. However, there are certain drawbacks to using nanoparticles for photocatalysis, such as their high band gap and the requirement that the photocatalyst's band gap must match the energy of the visible light photons in order to achieve effective visible light photocatalysis. Unfortunately, many metal oxide nanoparticles have a band gap that corresponds to ultraviolet (UV-Vis) light, thereby limiting their visible light photocatalytic activity. During the photocatalysis process, nanoparticles may agglomerate, which results in a decrease in the surface area as well as limiting the reaction-active sites that are available. This aggregation can occur due to various factors, such as a high concentration, pH changes, or the presence of impurities [16]. To overcome this limitation, researchers have developed various strategies, such as doping, surface modification, and band gap alteration, to activate metal oxide nanoparticles under visible light illumination. These modifications enable the nanoparticles to absorb a broader range of light, including visible light, thereby improving their photocatalytic efficiency [17]. Numerous transition metal oxide, such as ZnO, TiO₂, NiO, and CuO, and metal chalcogenides, such as ZnS and MoS₂, have been used for the removal of colored dye, industrial pollutants and pharmaceutical water waste [18–20]. The mostly studied transition metal oxide for the photocatalytic degradation of contamination as well as dye is TiO₂, which has a strong oxidizing power, is non-toxic, and is extremely stable toward both photo and chemical corrosion. Photocatalysis is a promising method because it is inexpensive and environmentally friendly. TiO₂ has a 3.2 ev band gap and absorbs wavelengths between 360 and 380 nm in the UV-Vis region. Several studies show the decreased band gap of TiO₂ by the doping of novel transition metals such as Cu, Ag, Au, Pt, Ni, and Co, as well as polyaniline (PANI), polypyrrole (PPY) and reduced graphene oxide, which extends the spectral shift in the visible region and increases the photocatalytic activity of TiO2 [21]. It has been shown that methyl blue (MB) and methyl orange (MO) exhibit 96.3% and 97% degradation under UV-Vis light irradiation using TiO₂ synthesized by the modified solvothermal method. Lin et al. [22] demonstrated the photocatalytic degradation (UV-VIS) of toxic 2-chlorophenol by using a TiO₂ catalyst. Similarly, Zhang et al. [23] investigated the photoelectric effect and photocatalytic properties of TiO₂ by doping it with Ag nanoparticles to enhance the photoelectric and photocatalytic degradation. Mingxuan Sun et al. [24] showed much improved visible

region photocatalytic activity, photochemical stability, and low charge recombination from TiO₂ doped with CdS and CdS/MoS₂.

On the basis of the above discussion, we have synthesized ternary composites of $Ag@Cu/TiO_2$ by the in situ solvothermal method for the photocatalytic degradation of RB dye in the visible region of light. The synthesized ternary composite $Ag@Cu/TiO_2$ was characterized for the structural and morphological characteristics. Finally, the photocatalytic degradation of RB dye and the hydrogen evolution phenomenon in the visible region were deeply investigated.

2. Experimental Section

2.1. Materials and Methods

Titanium (IV)-iso-propoxide (TIP) 97% from Qualigens, copper (II) sulphate pentahydrate 99.5% (CuSO₄.5H₂O) from Sisco Research Laboratories, silver nitrate 99.8% (AgNO₃) from Sigma Aldrich, ascorbic acid 99.7% from Sisco Research Laboratories, sodium borohydride 98% (NaBH₄) from Sisco Research Laboratories, hydrochloric acid 35% (HCl) from Sisco Research Laboratories (Mumbai, India) and rose bengal (RB) dye from Sigma Aldrich (St. Louis, MO, USA) were used in this study. Deionized water was used as the reaction medium for the synthetic procedure.

Field emission scanning electron microscopy (JEOL, JSM-7600F, FESEM, Tokyo, Japan) was used to study the surface morphology and elemental compositions. Transmission electron microscopy (JEOL, JSM, ARM-200F, HRTEM, Tokyo, Japan) was also used. The elemental mapping was recorded using an energy dispersive X-ray spectroscope (EDS) from Oxford Instruments, Oxfordshire, UK, equipped with FESEM. For the elemental detection, X-ray photoelectron spectroscopy (XPS) (ESCALAB 250 from Thermo Fisher Scientific, Warrington, UK) was used at a monochromatized Al K α X-ray source λ 1/4 1486.6 eV.

2.2. Synthesis of Ag@Cu/TiO₂

The synthesis of Ag@Cu/TiO₂ was performed by the solvothermal methodology. In this method, 6 mL of isopropanol was dispersed in 86 mL of water, and to it, 6 mL of HCl was added dropwise. To the isopropanol and acid mixture, 5 mL of TIP was slowly added, and the entire mixture was put under stirring conditions at 80 °C for 1 h, thereby resulting in a white colloidal solution (termed solution A). This white colloidal solution was subjected to centrifugation and subsequently the collected TiO₂ was washed with an excess of solvents (water and ethanol mixture) and finally dried in an air oven at 80 °C for 6 h to obtain pure TiO_2 . The Cu/TiO_2 was prepared by dissolving 0.4 g of $CuSO_4.5H_2O$ in 100 mL (for ~5% loading of Cu on TiO₂) of water and using 0.05 M NaOH to keep the pH at 12. To the above solution of CuSO₄.5H₂O, 30 mL of 0.05 M ascorbic acid was mixed dropwise and the resultant was heated at 60 °C with continuous stirring for 1 h (Figure 1). The yellow color of the mixture slowly changed to brown, indicative of the formed Cu (the Cu dispersion was termed solution B). Ultimately, both the solutions (A and B) were mixed under continuous stirring and the resultant Cu/TiO₂ was subjected to centrifugation, washed with an excess of solvents (water and ethanol) and finally dried at 80 °C for 6 h to obtain Cu/TiO₂. The Ag@Cu/TiO₂ was prepared by first preparing the colloidal solution of Ag nanoparticles by dissolving 0.12 g of AgNO₃ in 100 mL H₂O and then 30 mL of 0.06 M NaBH₄ was added to it dropwise. The Cu/TiO₂ binary composite was added to the Ag colloidal solution and the entire mixture was continuously stirred for 2 h. Thus, the prepared Ag@Cu/TiO2 composite was washed with an excess of solvents (water and ethanol) and finally dried at 80 °C for 6 h to obtain pure Ag@Cu/TiO₂.

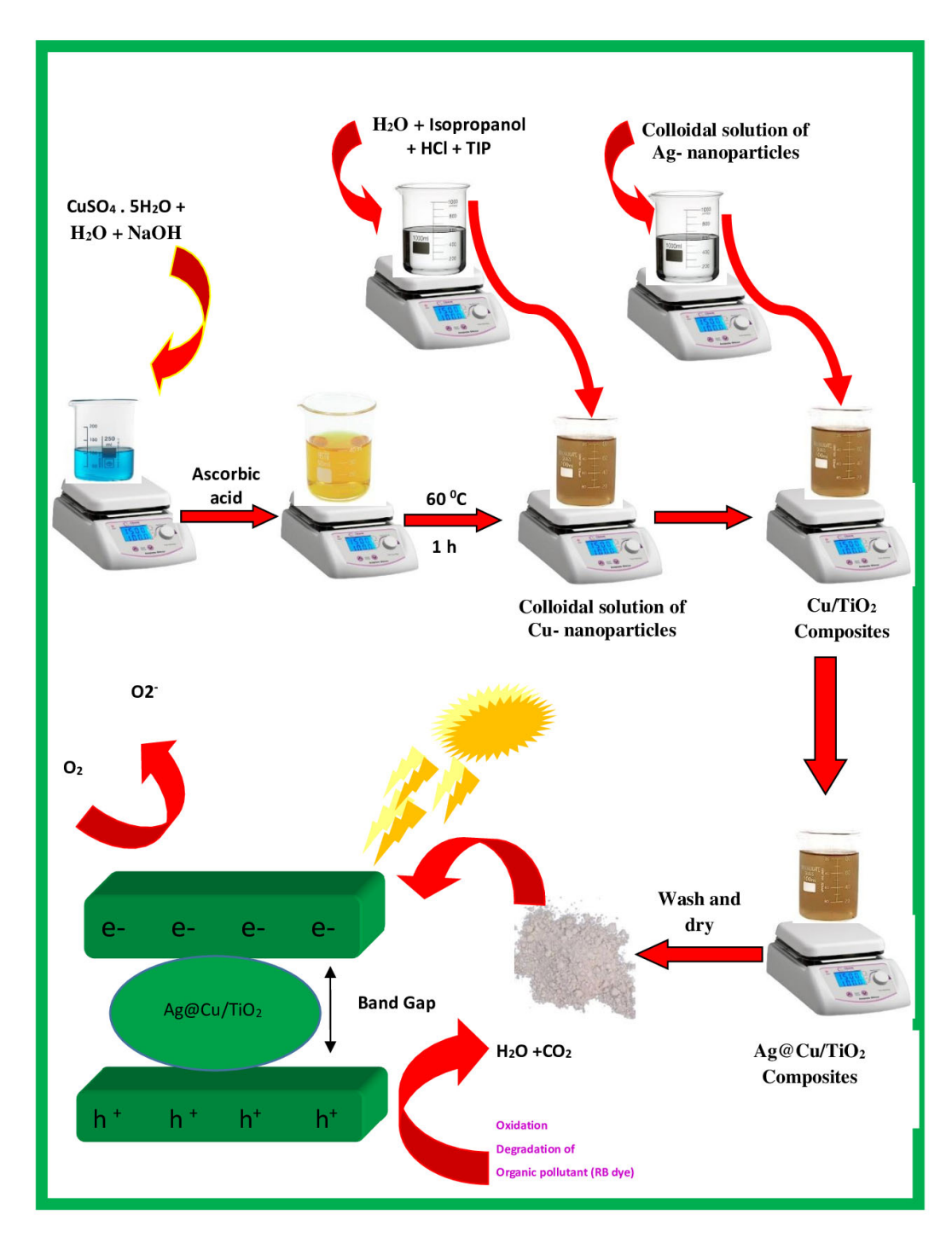


Figure 1. Schematic illustration of the synthesis of Ag@Cu/TiO₂.

2.3. Photocatalytic Degradation of RB and Hydrogen Production

The photocatalytic activity of the synthesized catalysts, namely pure TiO_2 , Ag/TiO_2 , Cu/TiO_2 , and $Ag@Cu/TiO_2$, was investigated by assessing their effectiveness in degrading RB dye. For this, 200 mg of prepared catalyst was mixed with a 250 mL solution containing 30 mg/L of RB dye and the pH was adjusted to 8. To attain adsorption—desorption equilibrium, the mixture was agitated for 30 m in the dark (refer to Supplementary Figure S4). Afterwards, visible light irradiation was performed using a 500 W halogen lamp. The solutions were collected at various intervals (0, 20, 40, and 60 min), followed by centrifugation and evaluation of the catalytic RB dye degradation using double-beam UV–Vis spectroscopy.

The degradation efficiency of the pure TiO₂, Ag/TiO₂, Cu/TiO₂, and Ag@Cu/TiO₂ was calculated through the following equation [25].

Degradation(%) =
$$\left(\frac{C_o - C_t}{C_o}\right) 100$$
 (1)

In the provided equation, C_0 represents the initial concentration of RB dye, while C_t signifies the concentration of RB after a specific time interval (0, 20, 40, and 60 min). Afterwards, the apparent rate constant (k) was determined using the following equation.

$$\ln\left(\frac{C_{t}}{C_{o}}\right) = -kt$$
(2)

To evaluate the hydrogen production, methanol was used as a scavenger. In hydrogen production processes, scavengers play a critical role in boosting efficiency. They tackle key challenges by capturing electron–hole pairs and preventing them from wasting generated energy [1]. Additionally, scavengers selectively target and eliminate molecules involved in undesired side reactions, protecting the crucial intermediates needed for hydrogen evolution. Furthermore, they can facilitate the movement of photogenerated charges within the system, ensuring their efficient utilization for hydrogen production. Essentially, scavengers act as guardians, optimizing various aspects of the process to maximize the hydrogen output [2].

3. Result and Discussion

3.1. Surface Morphological Analysis

The morphological analysis of the TiO_2 , Ag/TiO_2 , Cu/TiO_2 and $Ag@Cu/TiO_2$ was performed by SEM (Figure 2) and TEM (Figure 3). The SEM of the pure TiO_2 shows clusters of small-sized round particles packed into small and big aggregates. The Ag/TiO_2 , Cu/TiO_2 and $Ag@Cu/TiO_2$ show similar morphology, with all the constituents in the nano range. It can be predicted from the micrographs that all the constituents in the $Ag@Cu/TiO_2$ are well intercalated with each other. The TEM images of the $Ag@Cu/TiO_2$ show that all the TiO_2 , TiO_3 and TiO_4 are well intercalated with each other, with the size of some TiO_4 being slightly over 100 nm.

The elemental analysis of the TiO_2 , Ag/TiO_2 , Cu/TiO_2 and $Ag@Cu/TiO_2$ by EDS shows the presence of Ti and O in the TiO_2 , Ti, O and Ag in the Ag/TiO_2 , Cu, Ti and O in the Cu/TiO_2 and Cu, Ti, O and Ag in the $Ag@Cu/TiO_2$, thereby depicting the successful formation of the composite as well as the absence of any impurities. The uniform distribution of the respective elements, as depicted by the mapping analysis (Figure 4), suggests the efficacy of the synthesis methodology.

3.2. Surface Compositional and Chemical Analysis

The elemental composition and functional groups of the prepared catalysts (pure TiO_2 , Ag/TiO_2 , Cu/TiO_2 , and $Ag@Cu/TiO_2$) were studied by X-ray photoelectron spectroscopy (XPS). The survey spectra (Figure 5a) provided insights into the surface elements, while the detected composition is illustrated in Figure 5b. The pure TiO_2 demonstrated a composition comprising 58.1% oxygen and 41.9% titanium. In the case of the Ag/TiO_2 , the elements were present in the percentages of 51.7% oxygen, 45.3% titanium, and 3.0% silver. Similarly, the incorporation of copper into the Cu/TiO_2 was confirmed, with a composition of 50.7% oxygen, 43.0% titanium, and 6.3% copper. The ternary nanocomposite, referred to as $Ag@Cu/TiO_2$, exhibited an elemental composition of 35.4% oxygen, 39.2% titanium, 16.7% silver, and 8.7% copper.

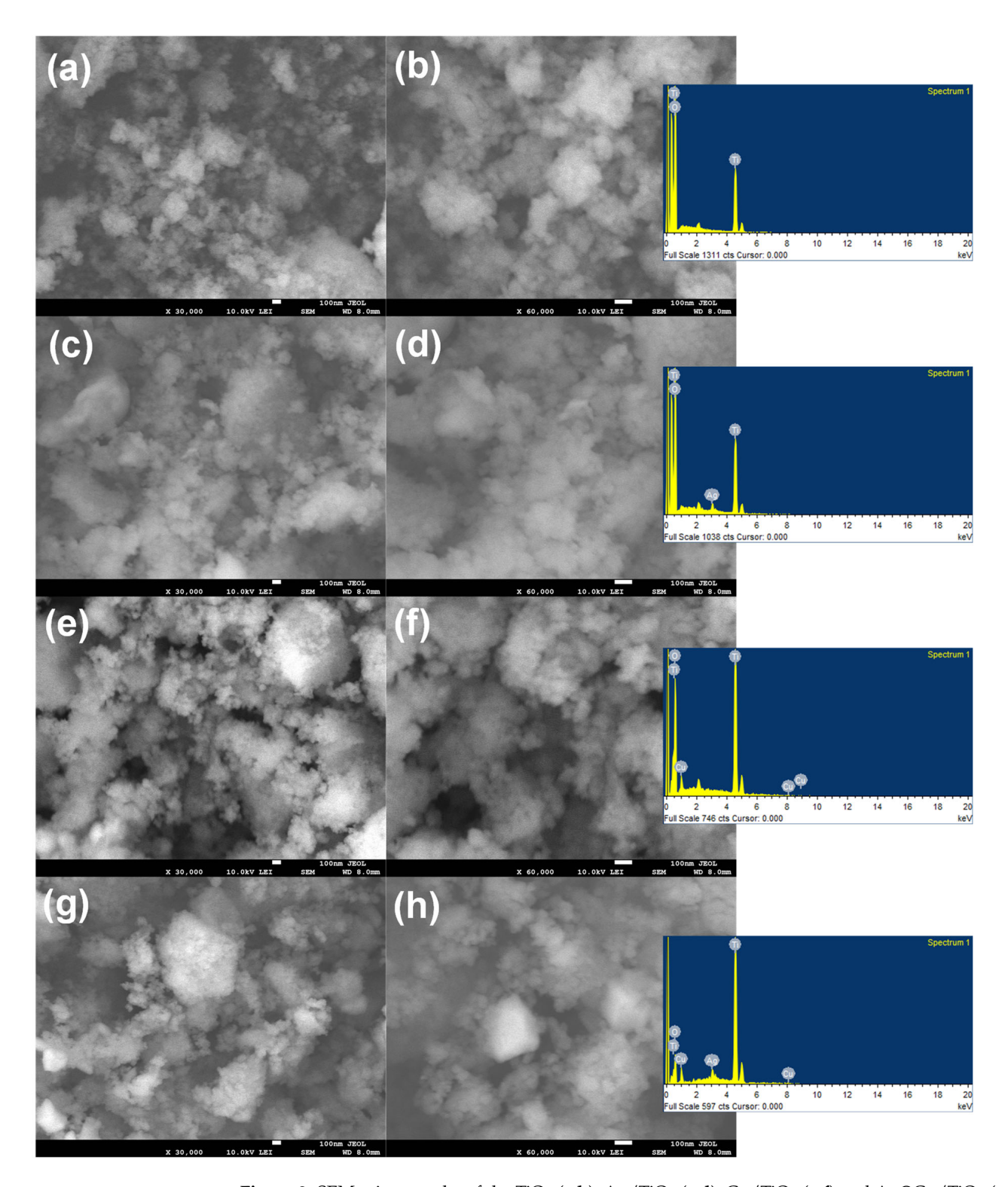


Figure 2. SEM micrographs of the TiO_2 (**a**,**b**), Ag/TiO_2 (**c**,**d**), Cu/TiO_2 (**e**,**f**) and $Ag@Cu/TiO_2$ (**g**,**h**), along with their respective elemental analysis.

The chemical state analysis of the Ti2p was further explored to elucidate the chemical interactions in the TiO₂, Ag/TiO₂, Cu/TiO₂, and Ag@Cu/TiO₂ (Figure 6a–d). In the chemical state analysis of the pure TiO₂ (Figure 6a), distinct peaks at 457.99 eV and 463.67 eV were observed, corresponding to Ti2p3/2 and Ti2p1/2, with contributions of 73.32% and 26.68%, respectively. The introduction of Ag and Cu into the TiO₂ resulted in alterations in the contributions of Ti2p3/2 and Ti2p1/2. Specifically, the Ag/TiO₂ sample exhibited

total contributions of 72.05% (Ti2p3/2) and 27.95% (Ti2p1/2). Similarly, the Cu/TiO₂ showed total contributions of 78.38% (Ti2p3/2) and 21.62% (Ti2p1/2). The final ternary composite, Ag@Cu/TiO₂, displayed total contributions of 72.31% (Ti2p3/2) and 27.69% (Ti2p1/2). In summary, the observed changes in the atomic percentage contributions of Ti2p3/2 and Ti2p1/2 in the pure TiO₂ following the addition of Ag and Cu signify the successful interaction between the components.

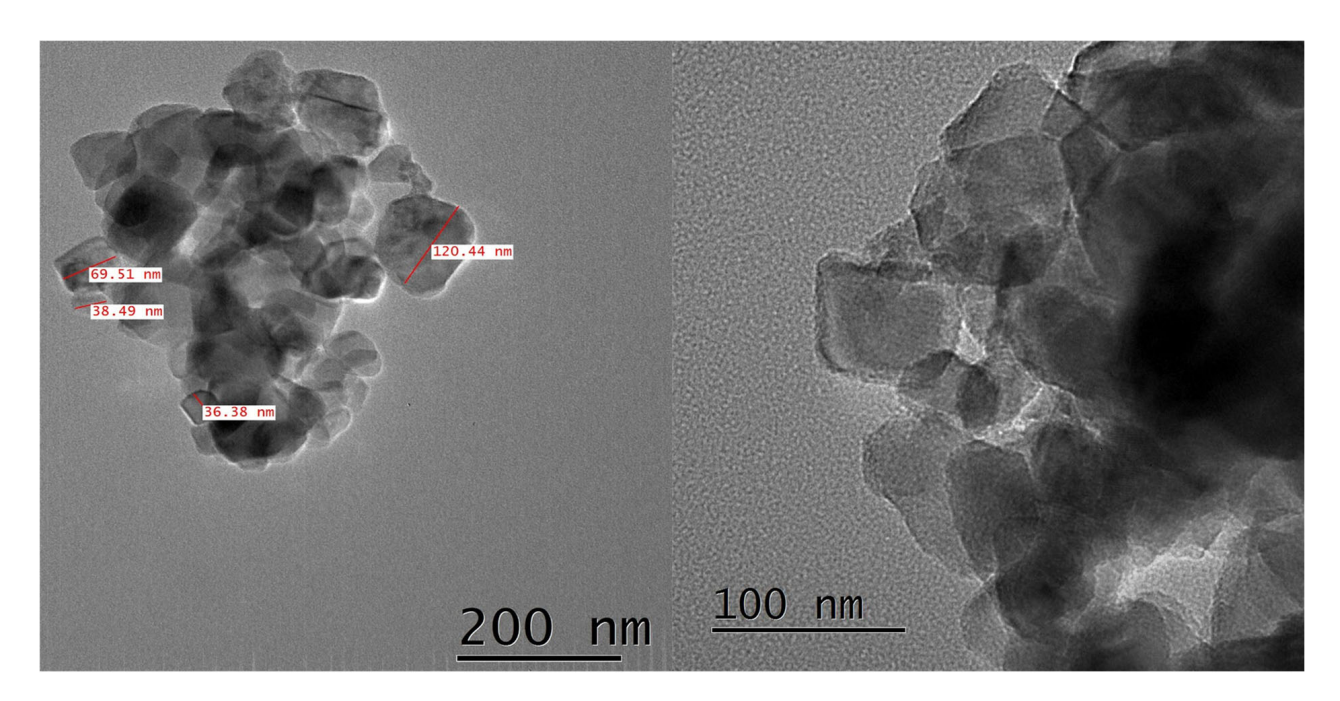


Figure 3. TEM images of the Ag@Cu/TiO₂ at different magnifications.

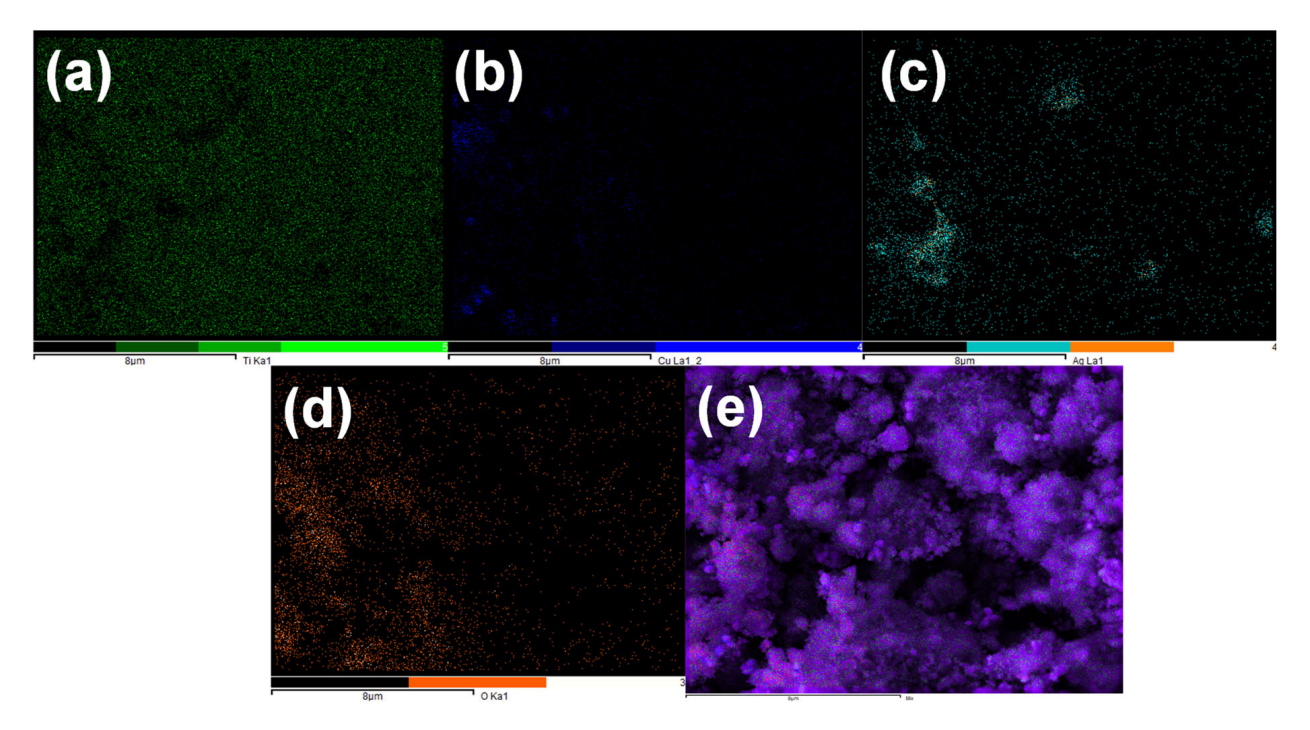


Figure 4. Elemental mapping distribution of the Ti (a), O (b), Ag (c), Cu (d) and mixed elements (e).

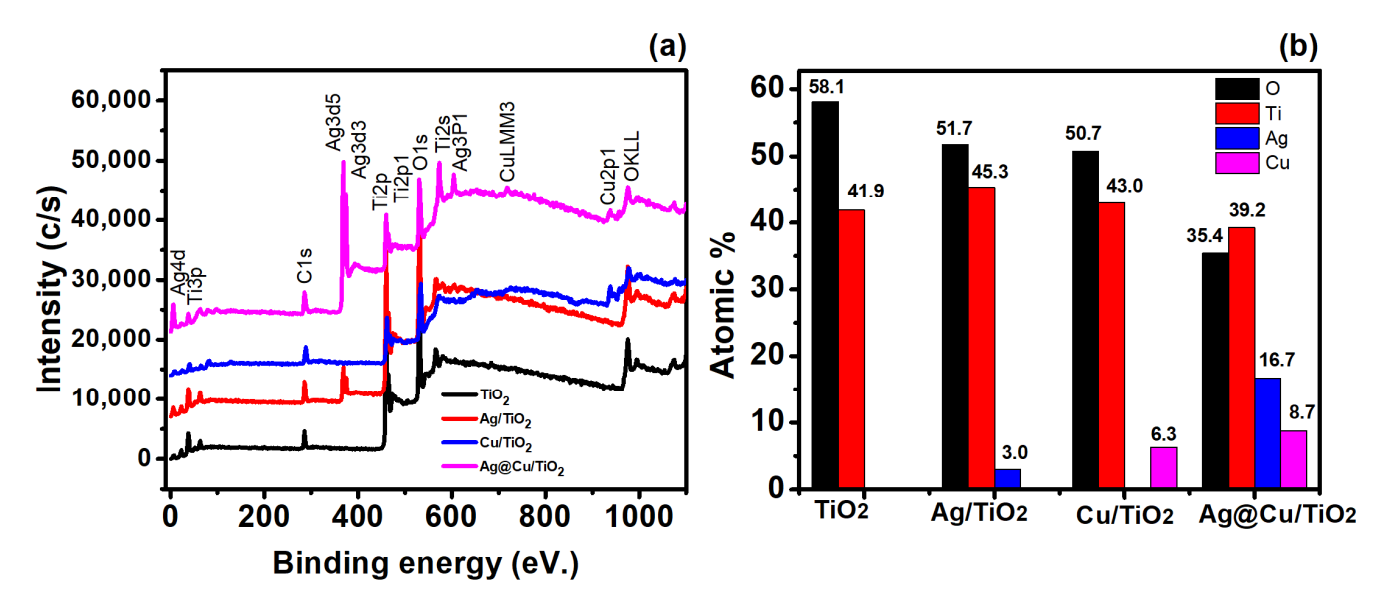


Figure 5. (a) XPS survey spectra and (b) composition of the TiO_2 , Ag/TiO_2 , Cu/TiO_2 and $Ag@Cu/TiO_2$.

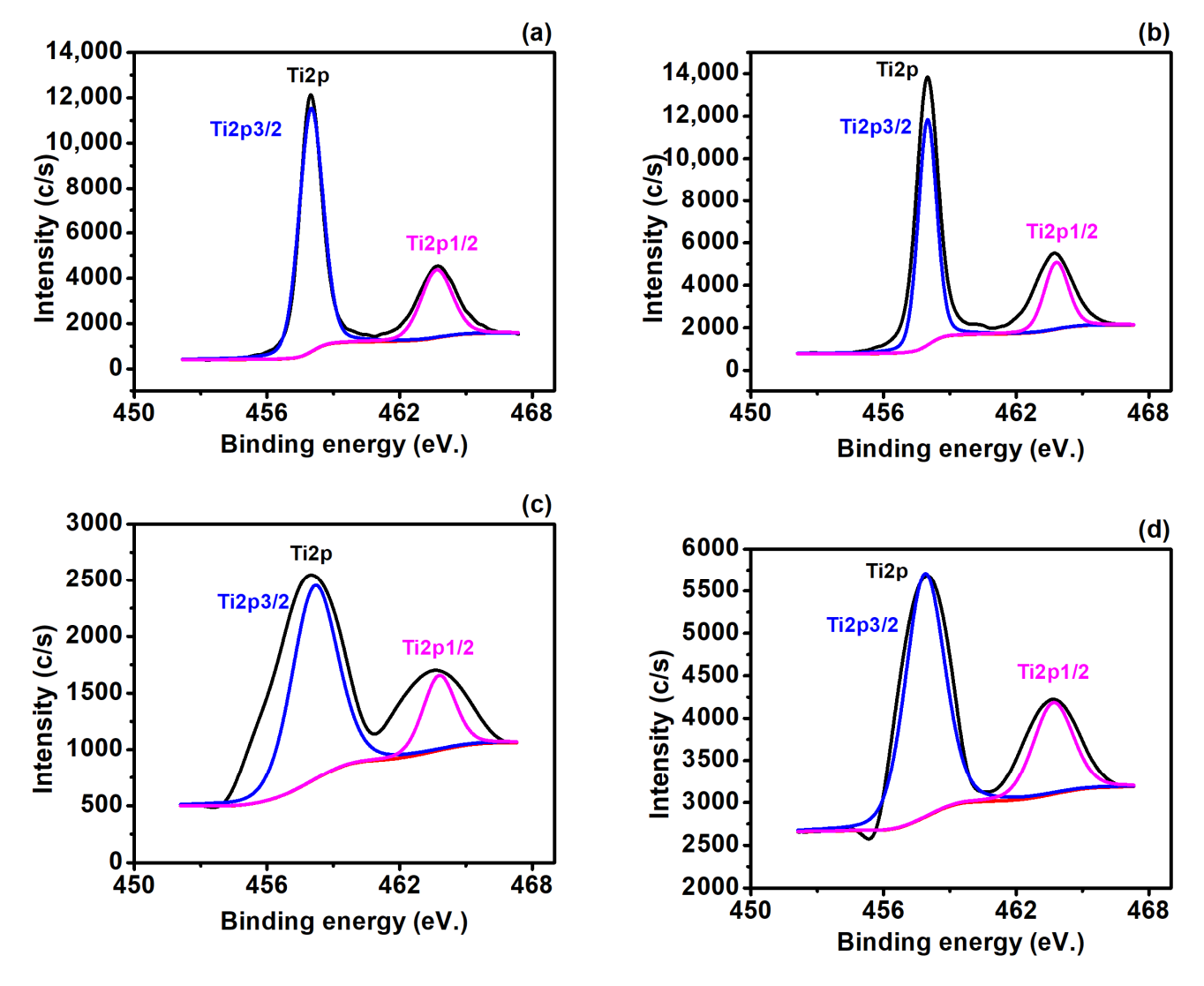


Figure 6. (a–d) High resolution spectra of the Ti2p for the TiO₂, Ag/TiO₂, Cu/TiO₂, and Ag@Cu/TiO₂.

The O1s spectra of the pure TiO_2 (Figure 7a) exhibit two main peaks at around 530 eV and 532.5 eV, attributed to the interaction between oxygen and Ti at 530 eV and oxygen vacancy at 532.5 eV, respectively [1]. Notably, the presence of Ag in the TiO_2 (Ag/ TiO_2), as depicted in Figure 7b, results in an increase in the oxygen vacancy from 12.54% to 13.12%. This trend continues with the addition of Cu to the TiO_2 (Cu/ TiO_2) and the ternary Ag@Cu/ TiO_2 . The maximum oxygen vacancy, reaching 56.45%, is observed for the Ag@Cu/ TiO_2 . These vacancies serve as active capture sites for dye molecules and pollutants, thereby enhancing the photocatalytic activity of the material [2]. These findings align with our photocatalytic results, as described later in Figure 9. Additionally, an extra peak is evident at around 534.6 eV for the Ag@Cu/ TiO_2 , attributed to the surface oxygen (Os), further contributing to the enhanced photocatalytic activity of the ternary Ag@Cu/ TiO_2 compared to the pure TiO_2 , Ag/ TiO_2 , and TiO_2 .

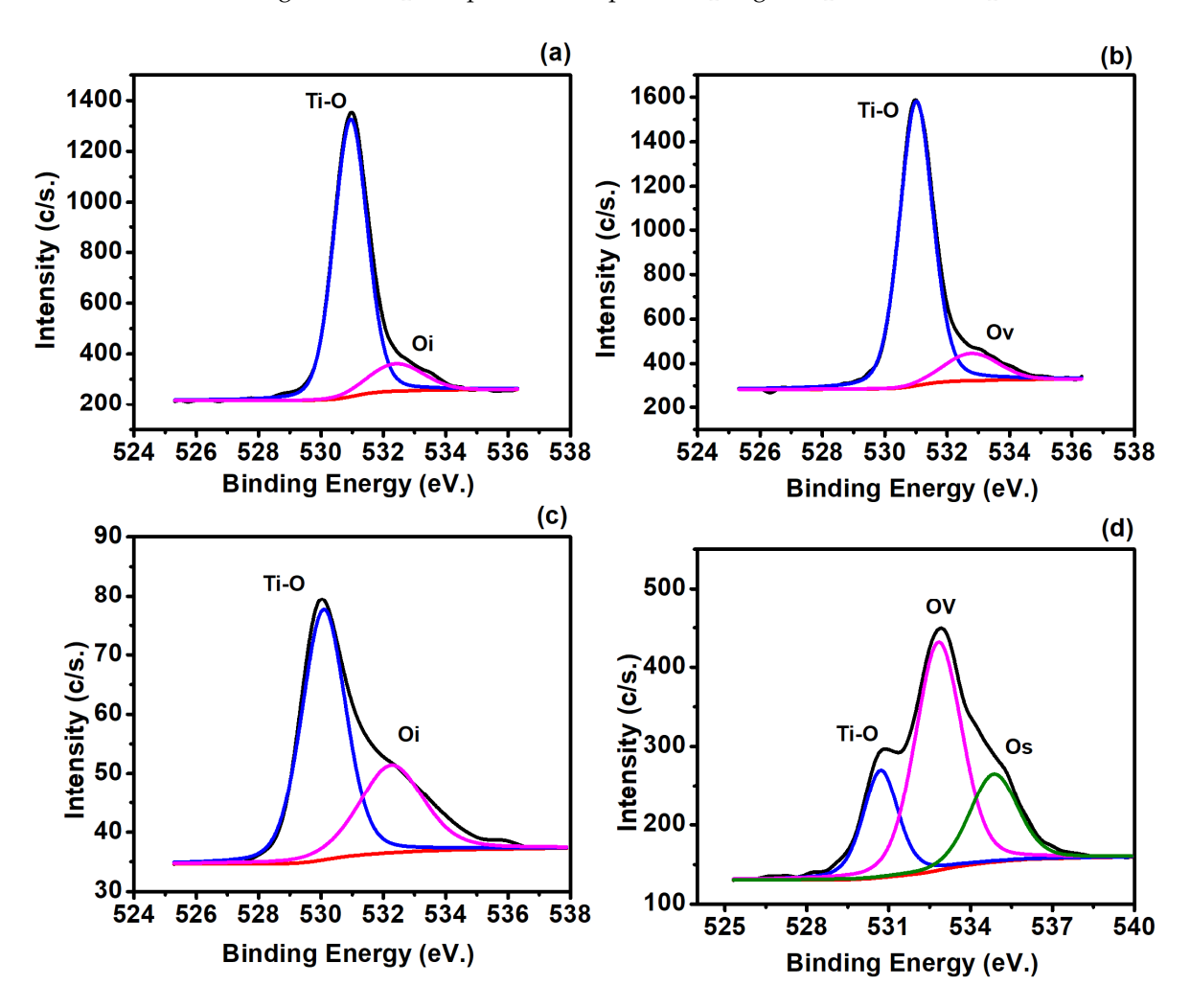


Figure 7. (a–d) O1s high resolution of the pure TiO_2 , Ag/TiO_2 , Cu/TiO_2 and $Ag@Cu/TiO_2$.

The chemical state of the Ag3d in the Ag/TiO₂ (Figure 8a) reveals peaks of Ag3d5/2 and Ag3d3/2 at 368 eV and 374 eV, respectively, with contributions of 59.90% and 40.10% [1]. However, upon the addition of Cu to the Ag/TiO₂ (Ag@Cu/TiO₂), as depicted in Figure 8b, these peaks undergo slight changes, with the percentages shifting to 59.03% and 40.97%, respectively. The Cu2p3 analysis of the Cu/TiO₂ and Ag@Cu/TiO₂ is presented in Figure 9c,d. The peaks observed at 937 eV are attributed to Cu's interaction with oxygen (CuOx), while those at 945.5 eV correspond to the shake-up satellite peak, with contributions of 27.46% and 30.71%, respectively [1]. This alteration in the contribution of the shake-up satellite peak further supports the enhancement of the photocatalytic activity of the ternary Ag@Cu/TiO₂.

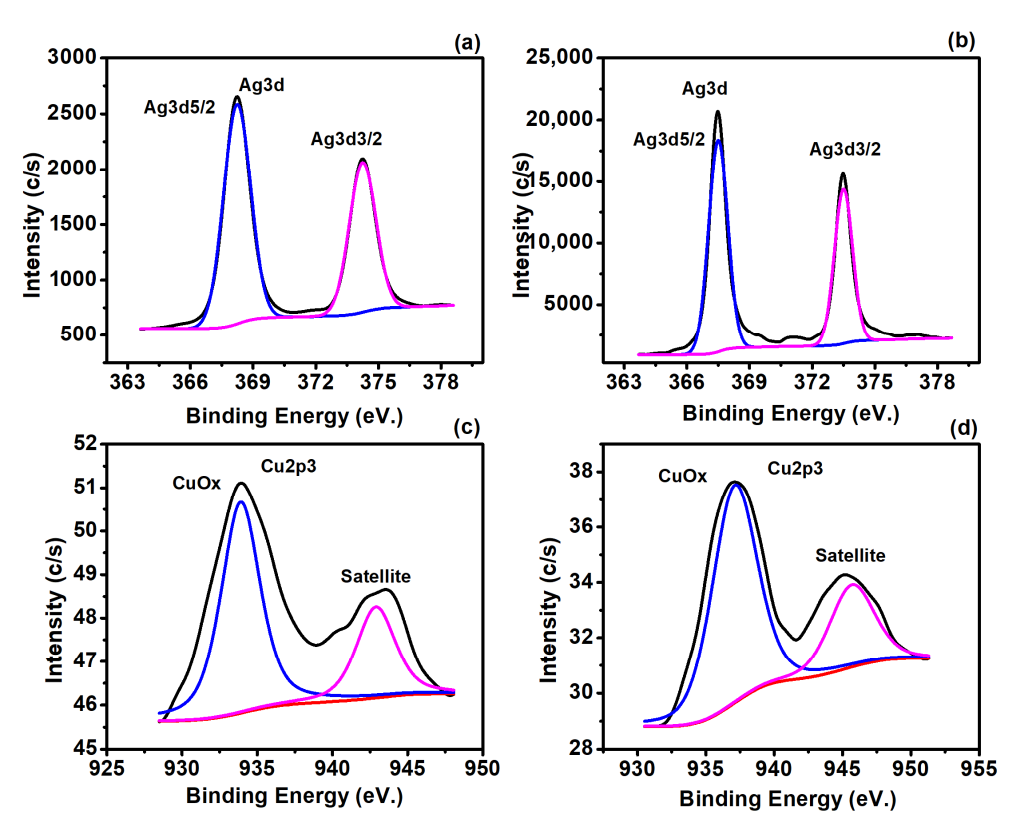


Figure 8. (a,b) Ag3d spectra of the Ag/TiO₂ and Ag@Cu/TiO₂, and (c,d) Cup3 analysis of the Cu/TiO₂ and Ag@Cu/TiO₂.

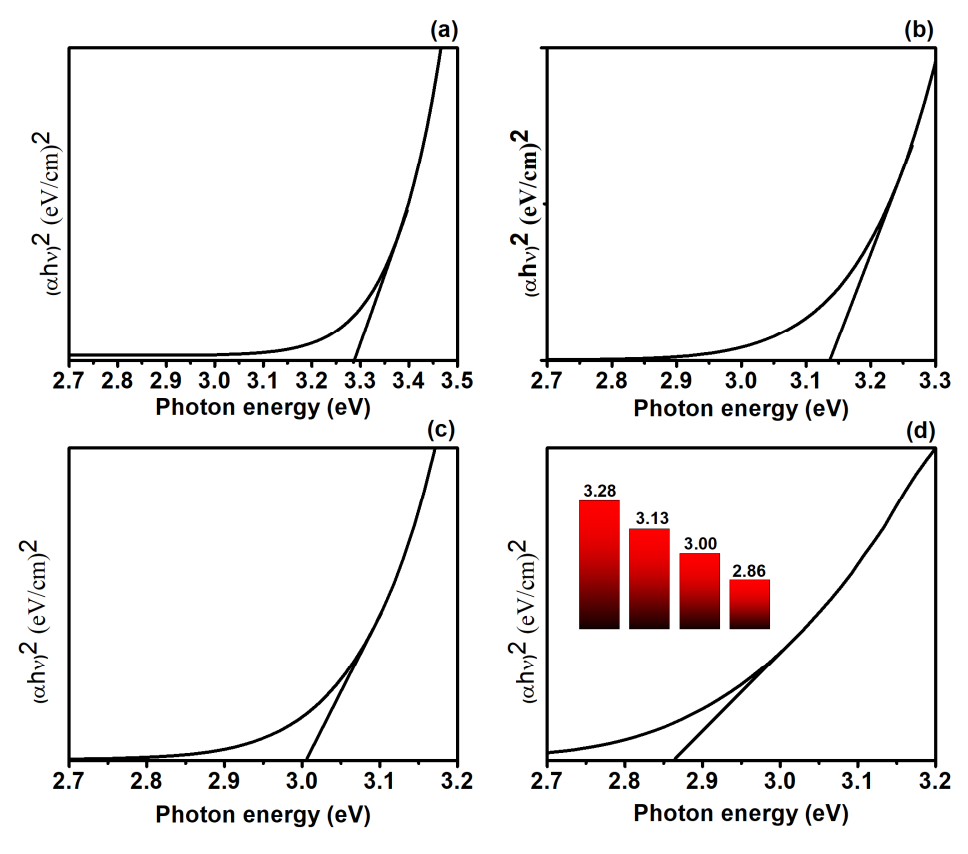


Figure 9. Band gap analysis of the (a) TiO_2 , (b) Ag/TiO_2 , (c) Cu/TiO_2 , and (d) $Ag@Cu/TiO_2$ and an inset showing the change in the band gap.

3.3. Charge Carrier Movement

The band gap alteration significantly influences the charge carriers' migration, directly effecting the photocatalytic efficiency of the catalyst. Therefore, the band gap calculations for the TiO_2 , Ag/TiO_2 , Cu/TiO_2 , and $Ag@Cu/TiO_2$ (Figure 9a–d) were determined using the Tauc plot relations [26].

$$\alpha(h\nu) = C(h\nu - E_g)^n$$

Here, C is a constant, hv represents the photon energy, and α is the absorption coefficient. The band gap of the pure TiO₂ measured at around 3.28 eV aligns well with the previously reported literature [27]. For the Ag/TiO₂ and Cu/TiO₂, the calculated band gap of 3.13 and 3.00 eV, respectively, indicates that the addition of Ag to both Cu and TiO₂ has a significant impact on the conduction of the charge carriers. This change in the TiO₂ band gap is attributed to the surface plasmon resonance effects [28]. The band gap of the Cu/TiO₂ is 3.00 eV, with a further reduction observed in the case of the Ag@Cu/TiO₂, measuring around 2.86 eV. The band gap reduction in the Ag@Cu/TiO₂ indicates the combined effects of Ag and Cu, contributing to the enhanced electron capture through the Schottky effect and surface plasmon resonance [29]. This synergistic effect results in a narrowed band gap, accelerated electrons and hole movements in the Ag@Cu/TiO₂, consequently resulting in the enhanced photocatalytic degradation of RB.

3.4. Charge Recombination Ratio

The charge recombination ratio is inversely proportional to the photocatalytic performance. The charge recombination ratios of the TiO_2 , Ag/TiO_2 , Cu/TiO_2 , and $Ag@Cu/TiO_2$ were determined through the photoluminescence spectra, as depicted in Figure 10. Analysis of the photoluminescence spectra revealed that the TiO_2 exhibited a peak of high intensity in comparison to the Ag/TiO_2 , Cu/TiO_2 , and $Ag@Cu/TiO_2$, indicating a high recombination ratio for the TiO_2 , consequently leading to lower photocatalytic efficiency. Conversely, the $Ag@Cu/TiO_2$ had a low intensity, suggesting a higher degradation efficiency. These photoluminescence results align with our photocatalytic findings, which indicated the degradation efficiency to be as follows: $Ag@Cu/TiO_2 > Cu/TiO_2 > Ag/TiO_2 > TiO_2$.

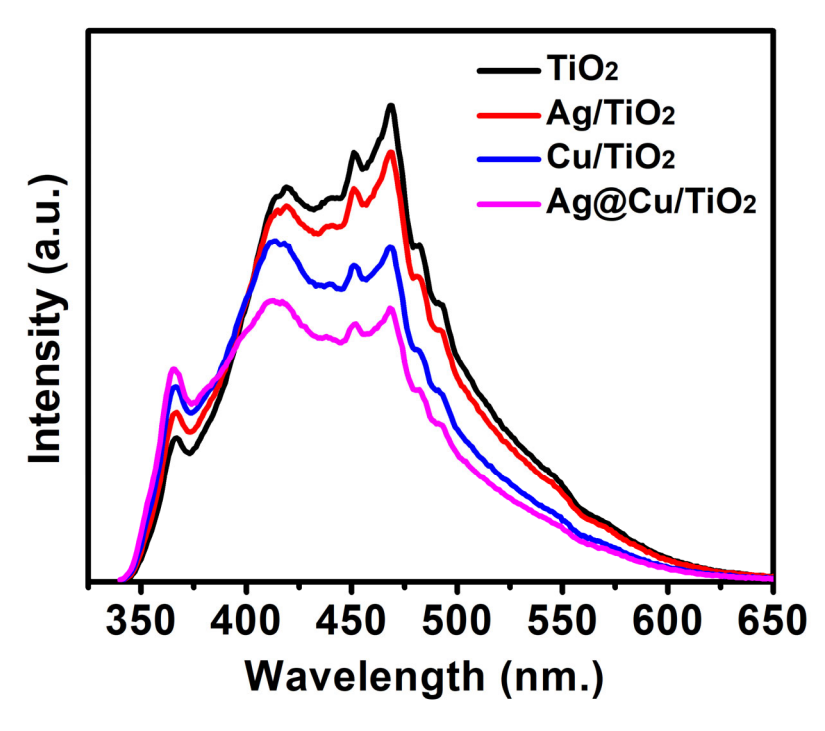


Figure 10. Charge recombination ratio of the TiO₂, Ag/TiO₂, Cu/TiO₂ and Ag@Cu/TiO₂.

3.5. Photocatalytic Degradation of RB

The time-dependent UV–Vis spectrum of RB under UV–Vis irradiation is depicted in Figure 9a, where the characteristic absorption peak is at λ max of 545 nm, which is the primary feature of RB. Observing Figure 9a, it becomes evident that with the increase in the irradiation time from 0 to 60 m, the absorption peak gradually diminishes, indicating the degradation of RB by the TiO₂, Ag/TiO₂, Cu/TiO₂, and Ag@Cu/TiO₂ under visible light.

Figure 9b,c illustrate the degradation statistics, demonstrating that the degradation efficiency of the pure TiO_2 is approximately 24.41% within 60 m of irradiation. This relatively low efficiency is due to its large band gap and high charge recombination rate. With the integration of Ag, the degradation efficiency of the pure TiO_2 increased to about 34.73% within the same duration. This enhancement is due to the surface photoluminescence resonance induced by silver, which suppresses the charge carriers' recombination, consequently intensifying the degradation of RB by the Ag/TiO_2 [25].

The degradation efficiency of the Cu/TiO₂ was approximately 68.38%, which is 2.82 times that of the pure TiO₂. This improvement is due to the reduced charge recombination ratio and the introduction of active sites such as oxygen vacancies in the pure TiO₂, resulting in the more effective capture of RB molecules and thus enhancing the degradation efficiency of the Cu/TiO₂ [26]. Similarly, the combined effect of silver and copper is evident in the photocatalytic efficiency of the ternary Ag@Cu/TiO₂, which exhibited a degradation rate of approximately 81.07%, which is 3.31 times that of the TiO₂. The notable improvement is due to the effective reduction in the recombination of the electron–hole pairs and the introduction of more active sites for RB molecule capture. Additionally, the incorporation of silver and copper into the TiO₂ led to heightened light absorption, further contributing to the overall enhancement. Moreover, as the degradation efficiency increases, the reaction rate constant of the TiO₂, Ag/TiO₂, Cu/TiO₂, and Ag@Cu/TiO₂ also increases. The reaction rate constant (Figure 11d) for the Ag@Cu/TiO₂ was found to be approximately 2.76×10^{-2} , 5.94 times than that of the TiO₂. The reaction rate constant for the Ag/TiO₂ and Cu/TiO₂ was around 7.11×10^{-3} and 1.91×10^{-2} , respectively.

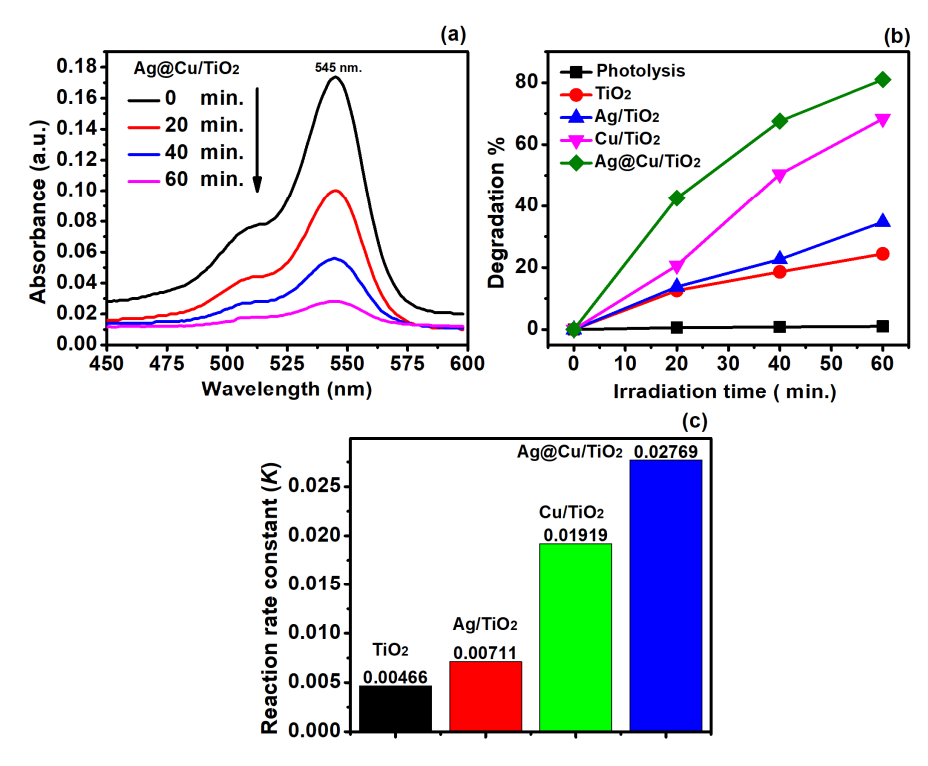


Figure 11. (a) Time-dependent UV–Vis spectrum of RB for the Ag@Cu/TiO₂, and (b) degradation statistics and (c) reaction rate constant of the TiO₂, Ag/TiO₂, Cu/TiO₂, and Ag@Cu/TiO₂ under the optimized value of 200 mg of each catalyst in a 250 mL solution containing 30 mg/L of RB dye.

3.5.1. Effect of RB Concentration

The dye concentration is a crucial factor as it can either enhance or diminish the photocatalytic efficiency of the catalyst. To examine this, a series of reactions were conducted at various concentrations of RB, namely 5, 20, 30, 40, and 50 ppm, while keeping the dosage of the Ag@Cu/TiO2 fixed at 200 mg/250 mL and the light intensity at a 500 W halogen lamp. As depicted in Figure 12a, the degradation of RB was found to be at its peak, around 81.07%, at an RB concentration of 30 ppm. The results revealed a progressive increase in the degradation rate from 5 ppm to 30 ppm, with degradation values of approximately 49.5%, 57.1%, 70.9%, and 81.07% for 5 ppm, 10 ppm, 20 ppm, and 30 ppm, respectively. Notably, the degradation of RB began to decline beyond 30 ppm, with degradation values of 75.9% and 65.2% for 40 ppm and 50 ppm, respectively. The highly efficient photocatalytic performance of the Ag@Cu/TiO2 is due to the growing availability of RB dye molecules for excitation and energy transfer with an increasing RB concentration [30]. However, upon surpassing a critical concentration level, in our case 30 ppm, the dye molecules begin to absorb the radiation instead of being absorbed by the Ag@Cu/TiO2, which results in a lowering of the photocatalytic efficiency of the Ag@Cu/TiO2 [31].

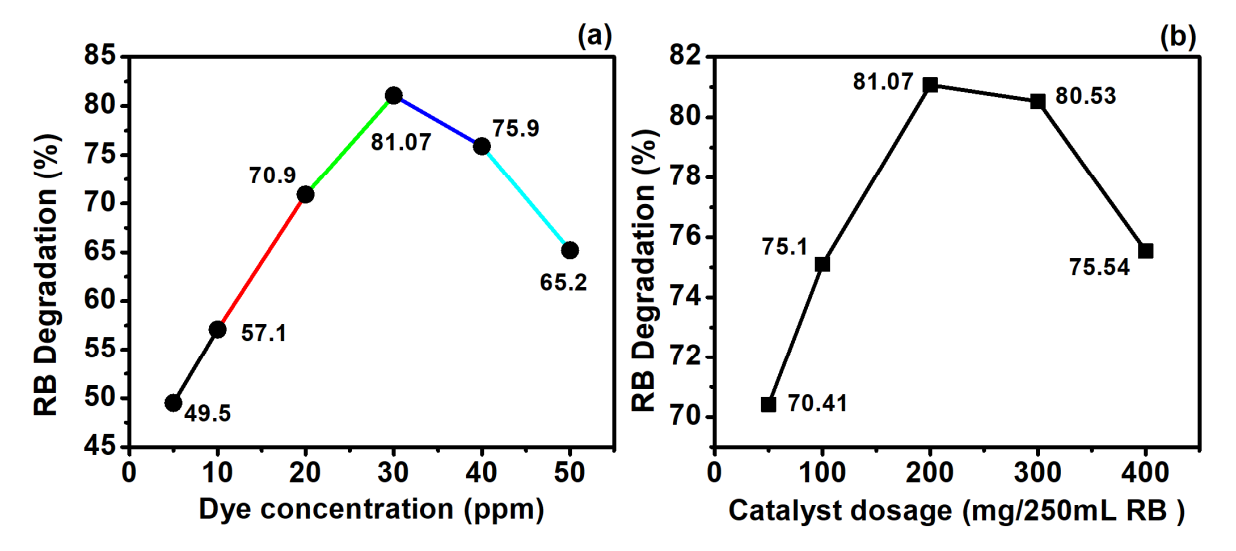


Figure 12. (a) Effect of the RB concentration at 5 ppm, 20 ppm, 30 ppm, 40 ppm, and 50 ppm while keeping the dosage of the $Ag@Cu/TiO_2$ fixed at 200 mg/250 mL and the light intensity at a 500 W halogen lamp. (b) Variation in the dosages of the $Ag@Cu/TiO_2$ at 50 mg/250 mL, 100 mg/250 mL, 200 mg/250 mL, 300 mg/250 mL, and 400 mg/250 mL.

3.5.2. Effect of Ag@Cu/TiO2 Dosage

The photocatalytic degradation depends on the quantity of the catalyst in the solution. For this, varying the amount of $Ag@Cu/TiO_2$ in the RB solution was studied for the purpose of photocatalysis. The dosages of the $Ag@Cu/TiO_2$ selected were 50 mg/250 mL, 100 mg/250 mL, 200 mg/250 mL, 300 mg/250 mL, and 400 mg/250 mL, while the irradiation time (0–60 m), irradiation light intensity (500 W), and RB concentration (300 ppm) were kept constant.

The results (Figure 12b) revealed that the efficiency of the Ag@Cu/TiO2 toward RB degradation increased with the increase in its dosage. Specifically, the efficiency was approximately 70.41% at 50 mg/250 mL, 75.1% at 100 mg/250 mL, and 81.07% at 200 mg/250 mL. This enhanced degradation efficiency might be due to the increased availability of active regions with the rise in the Ag@Cu/TiO2 dosage, facilitating the capture of RB molecules and intensifying the RB degradation

However, it was observed that as the dosage of the $Ag@Cu/TiO_2$ was increased from 200 mg/250 mL to 300 mg/250 mL, there was a slight reduction in the efficiency, which was approximately 80.53%. This efficiency further decreased to 75.54% at 400 mg/250 mL.

This decline in efficiency can be attributed to the desorption and scattering of light beyond a certain threshold dosage of Ag@Cu/TiO₂ [29].

The cyclic reusability of the $Ag@Cu/TiO_2$ was evaluated over seven consecutive cycles (see Figure S2). Remarkably, the reusability remained stable at 79.96% even after the seventh cycle. These findings underscore the promising potential of $Ag@Cu/TiO_2$ for RB dye degradation under visible light.

3.5.3. Proposed Photocatalytic Mechanism

Figure 13 depicts the suggested Ag@Cu/TiO₂ degradation pathway of RB. There are three possible ways for the formation of binary and ternary heterojunctions with TiO₂. The energy level of Cu's highest occupied molecular orbital is located between TiO₂'s valence band (VB) and conduction band (CB), which facilitates the formation of binary heterojunction. Under visible light irradiation, Cu/TiO₂ facilitates the hole transfer to Cu, leading to electron transport to the CB of the TiO2. The large number of holes in Cu react with RB, causing oxidation and subsequent RB degradation. Furthermore, the generated electrons degrade RB by reacting with the dissolved oxygen. Electron transfer from the TiO_2 to Ag's CB occurs in an $Ag@TiO_2$ binary heterojunction due to the differences in the TiO_2 's and Ag's work functions [32]. This shows that Ag has a significant role as an electron reservoir, reducing the charge recombination by creating a Schottky barrier. This, in turn, enhances the photocatalytic degradation under visible light [33]. Additionally, Ag's surface plasmon resonance (SPR) increases the photocatalytic activity by encouraging electron migration through photon harvesting. The hole migration to Cu facilitates the production of ternary heterojunctions in the Ag@Cu/TiO₂, where electrons are transferred to the CB of the TiO₂ and ultimately to the CB of the Ag. Here, they quicken the processes of oxidation and reduction, producing free radicals. The degradation process begins when RB absorbs these radicals.

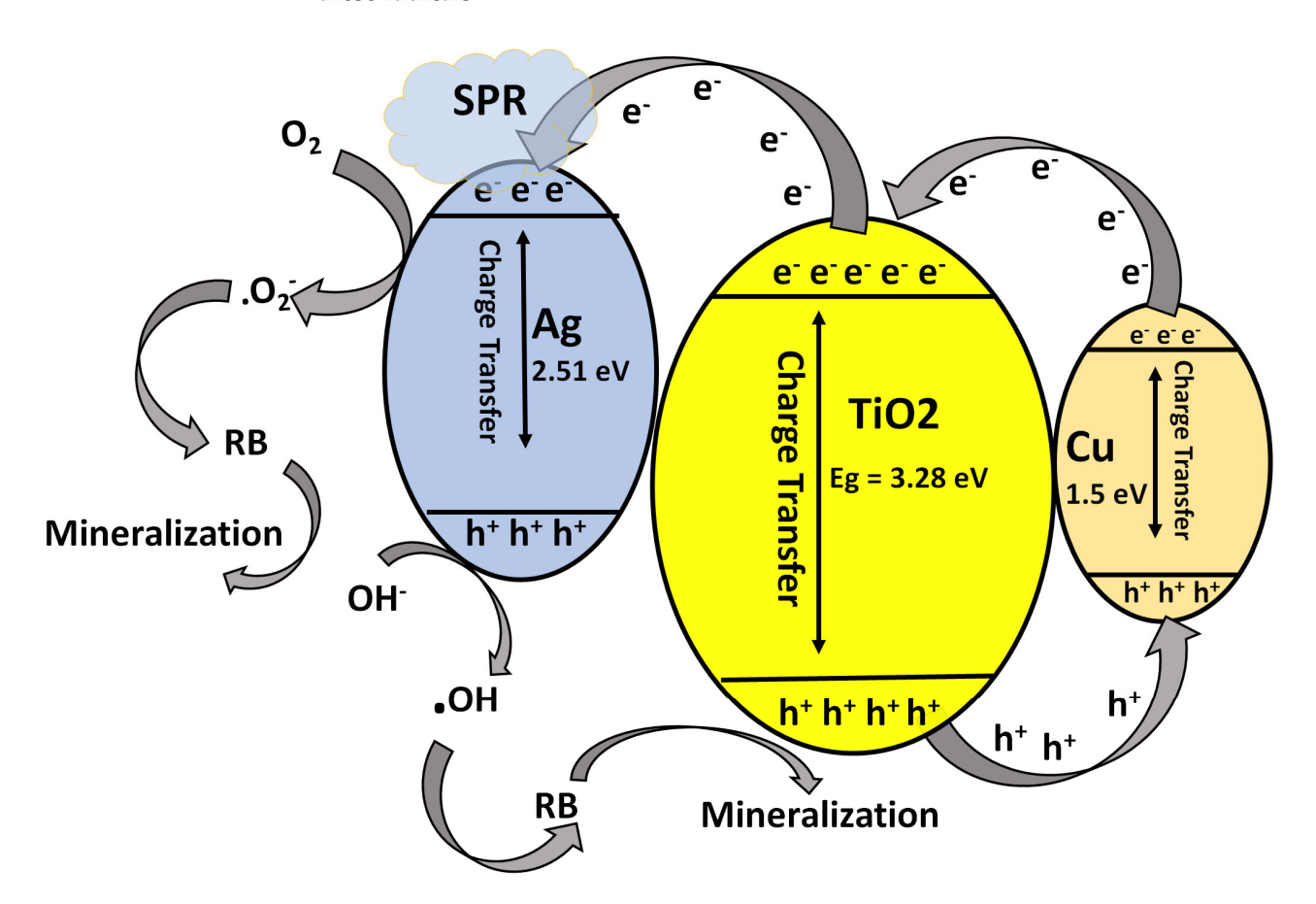


Figure 13. Proposed degradation mechanism of RB by Ag@Cu/TiO₂.

3.6. Hydrogen Production

Using a 20% concentration of methanol as a scavenger, we assessed the photocatalytic hydrogen generation of the TiO₂, Ag/TiO₂, Cu/TiO₂, and Ag@Cu/TiO₂. The outcomes, as shown in Figure 14, indicate that the pure TiO₂ exhibited a slower rate of hydrogen production (8.4 μ mol h⁻¹ g⁻¹), but the rate of hydrogen evolution in the Ag/TiO₂ increased significantly to 10.1 μ mol h⁻¹ g⁻¹ upon incorporation of Ag. This enhancement may be due to Ag's role in improving the charge carrier separation [34]. Moreover, it was observed that the Cu/TiO₂ had a superior capacity for hydrogen production compared to the Ag/TiO₂, with an approximate value of 14.4 μ mol h⁻¹ g⁻¹. The hydrogen production of the Ag@Cu/TiO₂ was found to be around 17.1 μ mol h⁻¹ g⁻¹, suggesting that Ag and Cu synergistically contribute to enhancing the hydrogen production of the pure TiO₂ [35]. Additionally, the XPS analysis of the O1s indicates a notable increase in the oxygen vacancies for the Ag@Cu/TiO₂ compared to the pure TiO₂, Cu/TiO₂, and Ag/TiO₂. This observation serves as another factor contributing to the enhanced hydrogen production.

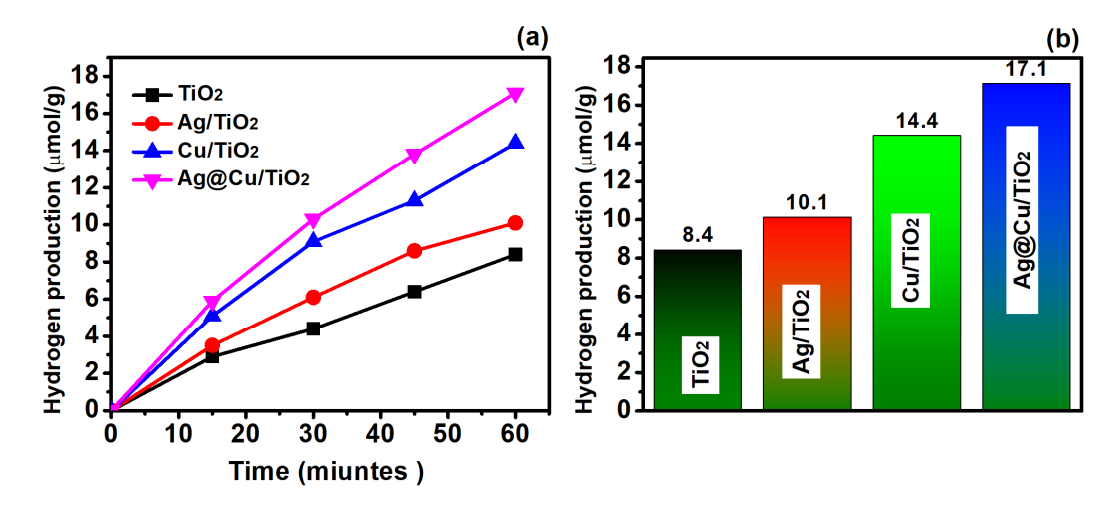


Figure 14. (a,b) Hydrogen production rate of the TiO₂, Ag/TiO₂, Cu/TiO₂, and Ag@Cu/TiO₂ with a 20% concentration of methanol as a scavenger.

4. Conclusions

In summary, ternary Ag@CuTiO2 nanocomposite was successfully synthesized by chemical methodology. The morphological and structural characterization showed that all the constituents were uniformly distributed, well intercalated and are in the nano range. The Ag@Cu/TiO2 showed a band gap of 2.86 eV in comparison to the pure TiO2 (3.28 eV), binary Ag/TiO2 (3.13 eV) and Cu/TiO2 (3.00 eV). The Ag@Cu/TiO2 displayed the lowest photoluminescence intensity, suggesting the highest degradation efficiency and lowest recombination rate. The photocatalytic degradation of RB by the Ag@Cu/TiO2 exhibited a degradation rate of ~81.07%, which is 3.31 times that of the TiO2. The reaction rate constant for the Ag@Cu/TiO2 was found to be 2.76 \times 10 $^{-2}$, i.e., 5.94 times that of the TiO2. Similarly, the reaction rate constant for the Ag/TiO2 and Cu/TiO2 was 7.11 \times 10 $^{-3}$ and 1.91 \times 10 $^{-2}$, respectively. Apart from this, the hydrogen production of the Ag@Cu/TiO2 was found to be 17.1 µmol h $^{-1}$ g $^{-1}$, suggesting that Ag and Cu synergistically contributed in enhancing the hydrogen production of the pure TiO2.

Supplementary Materials: The following supporting information can be downloaded at: https://www.mdpi.com/article/10.3390/chemistry6030028/s1, Figure S1: Reusability of Ag@Cu/TiO₂, Figure S2: UV data for (a) TiO₂, (b) Ag/TiO₂ (c) Cu/TiO₂ and (d) Ag@Cu/TiO₂, Figure S3: XRD pattern of TiO₂, Ag/TiO₂, Cu/TiO₂ and Ag@Cu/TiO₂. Figure S4a shows the degradation of RB using pure TiO₂ as the catalyst, while Figure S4b presents the UV absorbance data for the degradation of RB using pure TiO₂ under various pH levels, ranging from 7 to 9.

Author Contributions: Conceptualization, S.Y., A.J., P.K., S.A.A. and M.O.A.; Data curation, S.S. and S.Y.; Formal analysis, S.Y., S.S. and S.A.A.; Funding acquisition, S.Y. and P.K.; Investigation S.Y., A.J., P.K., S.A.A., M.O.A. and M.A.; Methodology, S.Y., P.K., A.J. and M.O.A.; Project administration, S.Y., A.J., P.K. and M.O.A.; Resources, S.Y., A.J., P.K. and M.O.A.; Software, S.S. and M.A.; Supervision, A.J., P.K. and M.O.A.; Validation, S.Y. and M.A.; Visualization, S.Y., P.K., S.A.A. and M.O.A.; Writing—original draft, S.Y. and M.A.; Writing—review & editing, S.Y., A.J., P.K. and M.O.A. All authors have read and agreed to the published version of the manuscript.

Funding: Both the authors (Pramod Kumar and Satish Yadav) would like to thank the Higher Education Department of the Uttar Pradesh Government (India) for providing financial assistance and fellowship through the Research and Development grant (Letter No. 89/2022/1585/सनर-4-2022/001-4-32-2022, dated 10/11/2022).

Data Availability Statement: The data will be made available upon request.

Acknowledgments: Both the authors (Pramod Kumar and Satish Yadav) would like to thank the Higher Education Department of the Uttar Pradesh Government (India) for providing financial assistance and fellowship through the Research and Development grant (Letter No. 89/2022/1585/सतर-4-2022/001-4-32-2022, dated 10/11/2022).

Conflicts of Interest: The authors declare no conflict of interest.

References

- 1. Feng, A.; Feng, J.; Xing, W.; Jiang, K.; Tang, W. Versatile Applications of Electrochemical Flow-through Systems in Water Treatment Processes. *Chem. Eng. J.* **2023**, 473, 145400. [CrossRef]
- 2. Huang, L.; Huang, X.; Yan, J.; Liu, Y.; Jiang, H.; Zhang, H.; Tang, J.; Liu, Q. Research Progresses on the Application of Perovskite in Adsorption and Photocatalytic Removal of Water Pollutants. *J. Hazard. Mater.* **2023**, 442, 130024. [CrossRef] [PubMed]
- 3. Noor, R.; Maqsood, A.; Baig, A.; Pande, C.B.; Zahra, S.M.; Saad, A.; Anwar, M.; Singh, S.K. A Comprehensive Review on Water Pollution, South Asia Region: Pakistan. *Urban Clim.* **2023**, *48*, 101413. [CrossRef]
- 4. Huang, S.-T.; Lee, W.W.; Chang, J.-L.; Huang, W.-S.; Chou, S.-Y.; Chen, C.-C. Hydrothermal Synthesis of SrTiO₃ Nanocubes: Characterization, Photocatalytic Activities, and Degradation Pathway. *J. Taiwan Inst. Chem. Eng.* **2014**, 45, 1927–1936. [CrossRef]
- 5. Solayman, H.M.; Hossen, M.A.; Abd Aziz, A.; Yahya, N.Y.; Hon, L.K.; Ching, S.L.; Monir, M.U.; Zoh, K.-D. Performance Evaluation of Dye Wastewater Treatment Technologies: A Review. *J. Environ. Chem. Eng.* **2023**, *11*, 109610. [CrossRef]
- 6. Beheshti, A.; Hashemi, F.; Behvandi, F.; Mayer, P.; Atzei, D. Selective High Adsorption Capacity for Congo Red Dye of a New 3D Supramolecular Complex and Its Magnetic Hybrid. *Inorg. Chem. Front.* **2018**, *5*, 694–704. [CrossRef]
- 7. Amiri, S.; Vatanpour, V.; He, T. Optimization of Coagulation-Flocculation Process in Efficient Arsenic Removal from Highly Contaminated Groundwater by Response Surface Methodology. *Molecules* **2022**, 27, 7953. [CrossRef] [PubMed]
- 8. Gan, Y.; Ding, C.; Xu, B.; Liu, Z.; Zhang, S.; Cui, Y.; Wu, B.; Huang, W.; Song, X. Antimony (Sb) Pollution Control by Coagulation and Membrane Filtration in Water/Wastewater Treatment: A Comprehensive Review. *J. Hazard. Mater.* **2023**, 442, 130072. [CrossRef] [PubMed]
- 9. Saeed, U.; Jilani, A.; Iqbal, J.; Al-Turaif, H. Reduced Graphene Oxide-Assisted Graphitic Carbon Nitride@ ZnO Rods for Enhanced Physical and Photocatalytic Degradation. *Inorg. Chem. Commun.* **2022**, *142*, 109623. [CrossRef]
- 10. Blázquez-Moraleja, A.; Moya, P.; Marin, M.L.; Bosca, F. Synthesis of Novel Heterogeneous Photocatalysts Based on Rose Bengal for Effective Wastewater Disinfection and Decontamination. *Catal. Today* **2023**, *413*, 113948. [CrossRef]
- 11. Flores, J.; Moya, P.; Bosca, F.; Marin, M.L. Photoreactivity of New Rose Bengal-SiO₂ Heterogeneous Photocatalysts with and without a Magnetite Core for Drug Degradation and Disinfection. *Catal. Today* **2023**, *413*, 113994. [CrossRef]
- 12. Shivaji, K.; Sridharan, K.; Kirubakaran, D.D.; Velusamy, J.; Emadian, S.S.; Krishnamurthy, S.; Devadoss, A.; Nagarajan, S.; Das, S.; Pitchaimuthu, S. Biofunctionalized CdS Quantum Dots: A Case Study on Nanomaterial Toxicity in the Photocatalytic Wastewater Treatment Process. *ACS Omega* 2023, *8*, 19413–19424. [CrossRef] [PubMed]
- 13. Lei, B.; Robertson, N. TiO₂ Mesocrystals: Immobilisation, Surface Fluorination and Application in Photocatalytic Water Treatment. *Appl. Surf. Sci.* **2023**, *616*, 156487. [CrossRef]
- Arabkhani, P.; Saeedi, N.; Sadeghi, H.; Nouripour-Sisakht, S.; Gharaghani, M.; Asfaram, A. Plant Extracts-Mediated Green Synthesis of Zinc Oxide/Carbon Nanofiber Nanocomposites with Highly Efficient Photocatalytic and Antimicrobial Properties for Wastewater Treatment. J. Water Process Eng. 2023, 54, 104020. [CrossRef]
- 15. Guo, M.; Yuan, B.; Sui, Y.; Xiao, Y.; Dong, J.; Yang, L.; Bai, L.; Yang, H.; Wei, D.; Wang, W.; et al. Rational Design of Molybdenum Sulfide/Tungsten Oxide Solar Absorber with Enhanced Photocatalytic Degradation toward Dye Wastewater Purification. *J. Colloid Interface Sci.* 2023, 631, 33–43. [CrossRef] [PubMed]
- 16. Christoforidis, K.C.; Fornasiero, P. Photocatalytic Hydrogen Production: A Rift into the Future Energy Supply. *ChemCatChem* **2017**, *9*, 1523–1544. [CrossRef]
- 17. Dong, S.; Feng, J.; Fan, M.; Pi, Y.; Hu, L.; Han, X.; Liu, M.; Sun, J.; Sun, J. Recent Developments in Heterogeneous Photocatalytic Water Treatment Using Visible Light-Responsive Photocatalysts: A Review. *RSC Adv.* **2015**, *5*, 14610–14630. [CrossRef]

18. Palanisamy, V.K.; Manoharan, K.; Raman, K.; Sundaram, R. Efficient Sunlight-Driven Photocatalytic Behavior of Zinc Sulfide Nanorods towards Rose Bengal Degradation. *J. Mater. Sci. Mater. Electron.* **2020**, *31*, 14795–14809. [CrossRef]

- 19. Tayeb, A.M.; Hussein, D.S. Synthesis of TiO₂ Nanoparticles and Their Photocatalytic Activity for Methylene Blue. *Am. J. Nanomater.* **2015**, *3*, 57–63.
- 20. Li, Z.; Meng, X.; Zhang, Z. Recent Development on MoS₂-Based Photocatalysis: A Review. *J. Photochem. Photobiol. C Photochem. Rev.* **2018**, 35, 39–55. [CrossRef]
- 21. Li, Z.; Wang, S.; Wu, J.; Zhou, W. Recent Progress in Defective TiO₂ Photocatalysts for Energy and Environmental Applications. *Renew. Sustain. Energy Rev.* **2022**, *156*, 111980. [CrossRef]
- 22. Chun-Te Lin, J.; Sopajaree, K.; Jitjanesuwan, T.; Lu, M.-C. Application of Visible Light on Copper-Doped Titanium Dioxide Catalyzing Degradation of Chlorophenols. *Sep. Purif. Technol.* **2018**, *191*, 233–243.
- 23. Zhang, H.; Wang, G.; Chen, D.; Lv, X.; Li, J. Tuning Photoelectrochemical Performances of Ag-TiO₂ Nanocomposites via Reduction/Oxidation of Ag. Chem. Mater. 2008, 20, 6543–6549. [CrossRef]
- 24. Sun, M.; Wang, Y.; Fang, Y.; Sun, S.; Yu, Z. Construction of MoS₂/CdS/TiO₂ Ternary Composites with Enhanced Photocatalytic Activity and Stability. *J. Alloys Compd.* **2016**, *684*, 335–341. [CrossRef]
- 25. Dustgeer, M.R.; Asma, S.T.; Jilani, A.; Raza, K.; Hussain, S.Z.; Shakoor, M.B.; Iqbal, J.; Abdel-wahab, M.S.; Darwesh, R. Synthesis and Characterization of a Novel Single-Phase Sputtered Cu₂O Thin Films: Structural, Antibacterial Activity and Photocatalytic Degradation of Methylene Blue. *Inorg. Chem. Commun.* **2021**, *128*, 108606. [CrossRef]
- 26. Jilani, A.; Iqbal, J.; Rafique, S.; Abdel-wahab, M.S.; Jamil, Y.; Al-Ghamdi, A.A. Morphological, Optical and X-ray Photoelectron Chemical State Shift Investigations of ZnO Thin Films. *Optik* **2016**, 127, 6358–6365. [CrossRef]
- Kumari, A.; Zaman, M.; Kumar, A.; Singh, V.R.; Ghosh, A.; Sahoo, S.K.; Rahaman, A.; Mandal, S.K.; Bhunia, S. An Alternative Approach to Study Photo-Catalytic Behavior of TiO₂ Using Synchrotron-Based Advanced Spectroscopic Techniques. *J. Mater. Eng. Perform* 2023, 32, 10391–10401. [CrossRef]
- 28. Shi, Y.; Li, L.; Xu, Z.; Guo, F.; Li, Y.; Shi, W. Synergistic Coupling of Piezoelectric and Plasmonic Effects Regulates the Schottky Barrier in Ag Nanoparticles/Ultrathin g-C₃N₄ Nanosheets Heterostructure to Enhance the Photocatalytic Activity. *Appl. Surf. Sci.* **2023**, *616*, 156466. [CrossRef]
- 29. Di, S.; Guo, S.; Wang, Y.; Wang, W.; Jung, Y.M.; Chen, L.; Wang, L. Surface Plasmon Resonance Effect on Charge Transfer in Ag@ Cu₂O-rGO Composites. *Mater. Chem. Phys.* **2023**, 301, 127621. [CrossRef]
- 30. Hanafi, M.F.; Sapawe, N. Effect of Initial Concentration on the Photocatalytic Degradation of Remazol Brilliant Blue Dye Using Nickel Catalyst. *Mater. Today Proc.* **2020**, *31*, 318–320. [CrossRef]
- 31. Reza, K.M.; Kurny, A.; Gulshan, F. Parameters Affecting the Photocatalytic Degradation of Dyes Using TiO₂: A Review. *Appl. Water Sci.* **2017**, *7*, 1569–1578. [CrossRef]
- 32. Mansfeldova, V.; Zlamalova, M.; Tarabkova, H.; Janda, P.; Vorokhta, M.; Piliai, L.; Kavan, L. Work Function of TiO₂ (Anatase, Rutile, and Brookite) Single Crystals: Effects of the Environment. *J. Phys. Chem. C* **2021**, *125*, 1902–1912. [CrossRef]
- 33. Huang, K.; Li, C.; Zheng, Y.; Wang, L.; Wang, W.; Meng, X. Recent Advances on Silver-Based Photocatalysis: Photocorrosion Inhibition, Visible-Light Responsivity Enhancement, and Charges Separation Acceleration. *Sep. Purif. Technol.* **2022**, *283*, 120194. [CrossRef]
- 34. Yadav, A.A.; Hunge, Y.M.; Kang, S.-W. Spongy Ball-like Copper Oxide Nanostructure Modified by Reduced Graphene Oxide for Enhanced Photocatalytic Hydrogen Production. *Mater. Res. Bull.* **2021**, *133*, 111026. [CrossRef]
- 35. Wu, D.; Liu, H.; Chen, J.; Liu, W.; Histand, G.; Wang, T. Cu NPs-Embedded Cross-Linked Microporous 3D Reduced Graphene Hydrogels as Photocatalyst for Hydrogen Evolution. *J. Colloid Interface Sci.* **2020**, *577*, 441–449. [CrossRef]

Disclaimer/Publisher's Note: The statements, opinions and data contained in all publications are solely those of the individual author(s) and contributor(s) and not of MDPI and/or the editor(s). MDPI and/or the editor(s) disclaim responsibility for any injury to people or property resulting from any ideas, methods, instructions or products referred to in the content.